remote sensing

MDPI

Article

# Remote Sensing of Glacier Change in the Central Qinghai-Tibet Plateau and the Relationship with Changing Climate

**Linghong Ke [1], Xiaoli Ding [1,*], Wenkai Li [2] and Bo Qiu [2]**

[1] Department of Land Surveying and Geo-Informatics, The Hong Kong Polytechnic University, Hong Kong 999077, China; kekehere@126.com

[2] Institute for Climate and Global Change Research, School of Atmospheric Sciences, Nanjing University, Nanjing 210023, China; wenkai@smail.nju.edu.cn (W.L.); qiuboqbo@126.com (B.Q.)

* Correspondence: lsxlding@polyu.edu.hk

Academic Editors: Qiusheng Wu, Charles Lane, Melanie Vanderhoof, Chunqiao Song, Magaly Koch and Prasad S. Thenkabail

Received: 21 October 2016; Accepted: 23 January 2017; Published: 29 January 2017

**Abstract:** The widely distributed glaciers over the Qinghai-Tibet Plateau (QTP) represent important freshwater reserves and the meltwater feeds many major rivers of Asia. Glacier change over the QTP has shown high temporal and spatial variability in recent decades, and the driving forces of the variability are not yet clear. This study examines the area and thickness change of glaciers in the Dongkemadi (DKMD) region over central QTP by exploring all available Landsat images from 1976 to 2013 and satellite altimetry data over 2003–2008, and then analyzes the relationships between glacier variation and local and macroscale climate factors based on various remote sensing and re-analysis data. Results show that the variation of glacier area over 1976–2013 is characterized by significant shrinkage at a linear rate of $-0.31 \pm 0.04$ km$^2$·year$^{-1}$. Glacier retreat slightly accelerated in the 2000s, and the mean glacier surface elevation lowered at a rate of $-0.56$ m·year$^{-1}$ over 2003–2008. During the past 38 years, glacier change in the DKMD area was dominated by the variation of mean annual temperature, and was influenced by the state of the North Atlantic Oscillation (NAO). The mechanism linking climate variability over the central QTP and the state of NAO is most likely via changes in the strength of westerlies and Siberian High. We found no evidence supporting the role of summer monsoons (Indian summer monsoon and East Asian monsoon) in driving local climate and glacier changes. In addition, El Niño Southern Oscillation (ENSO) may be associated with the extreme weather (snow storm) in October 1986 and 2000 which might have led to significant glacier expansion in the following years. Further research is needed to better understand the physical mechanisms linking NAO, ENSO and climate variability over the mid-latitude central QTP.

**Keywords:** glacier; Qinghai-Tibet Plateau; remote sensing; climate change; North Atlantic Oscillation

## 1. Introduction

A large number of mountain glaciers are present over the Qinghai-Tibet Plateau (QTP), providing an important contribution to water sources for the local environment and feeding many large rivers of Asia, including the Indus, the Yangtze and the Yarlung Tsangpo [1–4]. In the context of climate change over recent decades, many studies have reported distinct spatial variability of glacier change over the QTP [2,5–9]. Strong glacier thinning and retreat have been widely found over southeastern QTP, while many glaciers in the northwestern plateau have kept an equilibrium state or slightly advanced during recent decades. The contrasting glacier behaviors over the plateau have been suggested to be associated with the variability of precipitation changes over the monsoon-dominated southeast

and westerlies-dominated northwest [2]. However, over the mid-latitude central QTP where three major atmospheric circulation systems intersect (westerlies, the Indian monsoon (IM) and the East Asian Summer Monsoon (EASM)) [10], the main driving forces (temperature, precipitation and the seasonality) of recent glacier changes and the related atmospheric circulations remain unclear. The Tanggula Mountains in the mid-latitude central QTP are a pool of temperate glaciers which provide important water sources for the upstream areas of the Yangtze River, the longest river in China.

Investigations of the glacier–climate interaction over the plateau have been limited by inadequate observations on glacier changes. In-situ mass balance records are directly measured at stakes installed over the glacier surface [11], but they are limited to a few small, low-lying and accessible glaciers and may not represent the regional variability of glacier changes. At present, increasing satellite observations allow examination of various glacier parameters (length, area, elevation and velocity) and their changes over large areas and extended time periods. Remote sensing based estimates are indirect, and mostly require some sort of ground control or validation (e.g., [12,13]); they, however, offer a practical approach of obtaining a statistically representative sampling of glacier changes [14,15]. In particular, images acquired from Landsat satellite series, which have the longest observation records of the earth surfaces (from the mid-1970s to present) at a medium-high resolution (30 m–80 m), provide valuable information about the temporal evolution of glaciers. The number of Landsat scenes that can be used for examining glacier changes mainly depends on the availability of cloud-free images acquired at the end of ablation seasons. In addition, recent elevation observations from satellite laser altimetry ICESat (Ice, Cloud, and land Elevation Satellite), which are less sensitive to weather conditions, have shown potentials in estimating glacier mass balances based on surface elevation changes [5,16]. The relatively short period (spanning 2003–2009) and sparse spatial sampling over the mid-latitude regions limit the use of ICESat data for investigating long-term glacier changes in the mountainous central Asia. However, ICESat data provide valuable information about glacier surface elevation which is almost absent for many mountain glaciers and the repeated elevation measurements offer independent measurements of glacier changes. As validation of the remote sensing estimates is generally difficult without ground truth, the use of multi-source observations is a practical way to evaluate the reliability of the remote sensing results.

The regional climate systems over the mid-latitude central QTP can be rather complex because of the potential intersection of monsoon systems and the westerlies, which are also tele-connected with large-scale atmospheric circulations. Recent studies suggested that the Arctic amplification may impact on the mid-latitude weather patterns and extremes [17,18] and mid-latitude westerlies may drive climate variation and glacier variability in the monsoon affected areas of High Asia [19]. On large spatial scales, climate change over the QTP may also be tele-connected with hemispheric or global atmospheric circulations including North Atlantic Oscillation (NAO) and El Niño Southern Oscillation (ENSO) [20]. Previous studies suggested that ENSO influences climate over the southern QTP through the link of IM [21,22], while NAO is associated with climate fluctuations over the northern QTP through modulation of westerlies [20,23]. Whether such teleconnections exist over the mid-latitude central QTP and how they affect local climate and glacier variability remain unclear.

With a focus on the Dongkemadi (DKMD) region over central QTP, this study explores the evolution of the glaciers by deploying maximum number of remotely sensed observations from the Landsat imagery and estimating recent glacier surface elevation changes from ICESat data. Thereafter the control of the annual and seasonal climate conditions on glacier changes is analyzed by exploring time series of various local and large-scale climatic variables. In particular, we will discuss the possible relationships between local climate variations and large-scale atmospheric circulations including westerlies, the IM, and ENSO events.

## 2. Study Area

The studied glaciers are located in the DKMD region in the Tanggula Mountains over central QTP (Figure 1). The study region contains a total of 32 valley or cirque glaciers, including the Da

Dongkemadi (DDG) and Xiao Dongkemadi (XDG) glaciers, covering a total area over 80 km$^2$ according to the second China Glacier Inventory (CGI2) [24] (Figure 1). The glaciers, with the minimum elevation over 5000 m a.s.l., have relatively smooth surfaces without evident moraines. The DKMD region lies close to the boundary between the monsoon-affected south and the westerlies-dominated north [25]. For the QTP, the westerlies are split into two paths: one flowing to the east around 40°N and the other following along the southwest path around the southern edges of the plateau [2,26] (Figure 1). The semi-arid continental climate is characterized by a long cold season from October to April and a short warm season from May to September. Meteorological observations at 5600 m recorded on the XDG during 1992–1993 reveal that the annual mean air temperature and annual precipitation are −9.8 °C and 302 mm, respectively [27]. Referring to meteorological data at weather stations and the CN05 gridded dataset (introduced in the dataset section), we estimate that the long-term average precipitation in warm season (May to September) accounts for about 70% of the total annual precipitation (the statistics is based on 1976–2013). According to the thermal conditions and the characteristics of local climate, the DKMD glaciers are typical temperate glaciers [11] and can be categorized into the "summer accumulation" type.

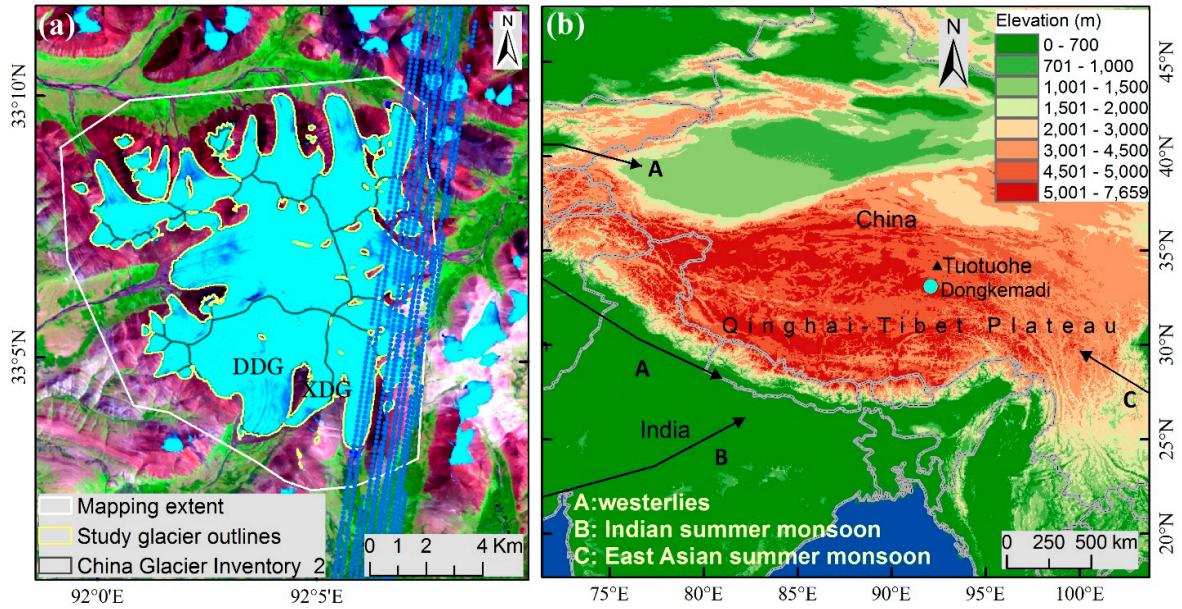


**Figure 1.** The study glaciers in the Dongkemadi (DKMD) region and the ICESat tracks (blue dots) shown on the false color composite of Landsat TM images (Bands 5, 4, and 2, for R, G, and B, respectively) (**a**); and the location of the study area in relation to three important atmospheric circulations in Asia (**b**). Glacier outlines in (**a**) are retrieved from the background TM images acquired on 30 August 2000.

## 3. Datasets and Methods

### *3.1. Glacier Area and Elevation Changes*

#### 3.1.1. Landsat Images over 1976–2013

We selected suitable Landsat scenes (Landsat MSS/TM/ETM+/OLI) which are available from the United States Geological Survey (USGS) for glacier mapping. Assuming no seasonal snow cover, snow/ice extent identified from the cloud-free Landsat imagery represents the glacierized area. To mitigate the influence of seasonal snow, we consider images acquired at the end of ablation season (late August to early September) as suitable for retrieving glacier outlines. A total of 21 Landsat images sampling 18 years from 1976 to 2013 were used in our glacier mapping (Table 1). All images, except

three acquired in 2001, 2003 and 2010 (marked in Table 1), are cloud-free over the glaciers. For these partly cloud-covered scenes, we used additional reference images (marked in Table 1) acquired in the same year to correct the cloud-affected parts. As there are few suitable images in the 1970s and early 1980s, we selected two images (1976 and 1986) whose acquisition dates do not strictly meet the requirement but are of high-quality in other aspects (cloud free and with minimal seasonal snow cover compared to other images acquired in the same year). Landsat ETM images acquired after 2003 (SLC-off) were not employed due to the presence of data gaps. We show false color composites of all used images in the supplementary material to illustrate the mapping conditions (Figure S1).

**Table 1.** List of Landsat images used in this study. Images marked with • are partly cloud covered and images marked with * were used for reference. The TM/ETM+/OLI and MSS images have a resolution of ~30 m and ~80 m, respectively.

| Sensor | Acquisition Date (YYYY/MM/DD) | Path/Row | Used Bands |
|---|---|---|---|
| Landsat 2/MSS | 1976/11/11 | 148/37 | 4, 5, 6, 7 |
| Landsat 5/TM | 1986/07/30 | 138/37 | 2, 4, 5 |
| Landsat 5/TM | 1988/07/28 | 137/37 | 2, 4, 5 |
| Landsat 5/TM | 1989/09/17 | 137/37 | 2, 4, 5 |
| Landsat 5/TM | 1990/08/19 | 137/37 | 2, 4, 5 |
| Landsat 5/TM | 1991/09/14 | 138/37 | 2, 4, 5 |
| Landsat 5/TM | 1992/08/31 | 138/37 | 2, 4, 5 |
| Landsat 5/TM | 1994/08/21 | 138/37 | 2, 4, 5 |
| Landsat 5/TM | 1995/08/17 | 137/37 | 2, 4, 5 |
| Landsat 5/TM | 2000/08/30 | 137/37 | 2, 4, 5 |
| Landsat 5/TM | 2001/07/23 • | 138/37 | 2, 4, 5 |
| Landsat 7/ETM+ | 2001/10/12 * | 137/37 | 2, 4, 5 |
| Landsat 5/TM | 2003/08/07 • | 137/37 | 2, 4, 5 |
| Landsat 5/TM | 2003/10/17* | 138/37 | 2, 4, 5 |
| Landsat 5/TM | 2004/09/10 | 137/37 | 2, 4, 5 |
| Landsat 5/TM | 2007/08/02 | 137/37 | 2, 4, 5 |
| Landsat 5/TM | 2009/08/30 | 138/37 | 2, 4, 5 |
| Landsat 5/TM | 2010/09/02 • | 138/37 | 2, 4, 5 |
| Landsat 5/TM | 2010/10/20 * | 138/37 | 2, 4, 5 |
| Landsat 5/TM | 2011/08/29 | 137/37 | 2, 4, 5 |
| Landsat 8/OLI | 2013/08/02 | 137/37 | 3, 5, 6 |

All images derived from the USGS are already processed to L1T products with standard terrain correction and are ready for further pixel-level analysis. We employed two well-established methods to extract glacier outlines from Landsat MSS and TM data respectively, given the different band specifications. For Landsat TM images, the semi-automated band ratio approach based on Normalized Difference Snow Index (NDSI) was used. NDSI is computed as the normalized difference of the reflectance of green band and short-wave infrared band (SWIR) [28]. An empirical threshold of 0.4 (based on examination of NDSI histogram around the study glaciers and tests on different thresholds) was chosen to segment the NDSI images into glacier area and non-glacier area. The mapping results are not sensitive to changes of the threshold partly because the contrasting bimodal distribution of NDSI value in the areas containing glaciers and non-glaciers. As shown in Figure 2, the absolute percent difference in the total mapped glacier area between our choice of threshold and the thresholds in 0.35–0.45 is mostly within 0.8%. To retrieve glacier area from the MSS image without short-wave bands, we used the ISODATA unsupervised classification method that iteratively clusters pixels class using minimum distance techniques [29]. In this process, the scene was firstly clipped around the glacier region and then was classified into four classes based on all the four bands (Table 1) with up to four iterations. The classification result is shown in Figure S2 in the supporting material. Post-classification processing is important to maintain high-quality results [30]. Thus, we manually modified glacier

outlines under partly cloud-covered images by referring to cloud-free reference images (Figure S3), and corrected misclassifications due to shadow and water bodies. Small individual glaciers with area <0.02 km$^2$ were omitted as they might represent seasonal snow patches. We calculated a buffer of 15 m (half of the pixel size) around the glacier outlines, and the differences between the buffered area and glacier polygons vary in the range of 2.9% to 3.2%, which can be seen as a rough assessment of the mapping accuracy. The accuracy matched well with the uncertainty ~3% of semi-automated mapping methods reported in previous studies (e.g., [31,32]).

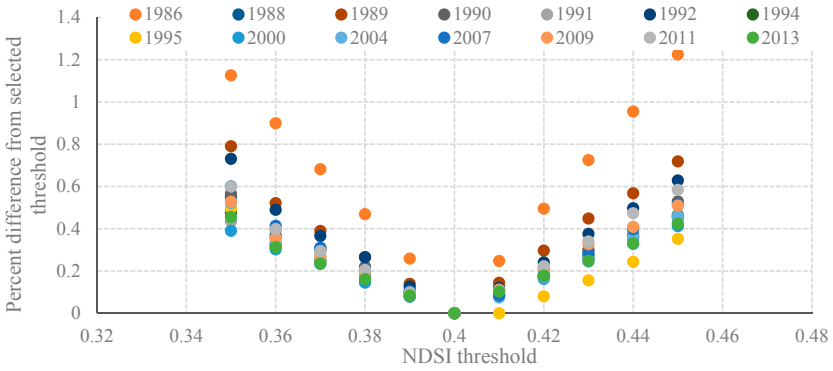


**Figure 2.** Glacier area sensitivity to the NDSI (Normalized Difference Snow Index) threshold for different years of analysis. Scenes with part cloud contamination as indicated in Table 1 are not included in this evaluation.

#### 3.1.2. ICESat Elevation Measurements over 2003–2008

Elevation measurements from level-2 ICESat Global Land Surface Altimetry Data product- GLA14 of release 33 [33] were used to estimate glacier surface elevation changes and the processing method was same to [34]. A total number of 14 repeated tracks (from March 2003 to November 2008) covered the glacier area (Figure 1). At each footprint, the elevation difference between ICESat and the SRTM DEM (dh in short thereafter) represents a measurement of the elevation change between the SRTM and the ICESat acquisition date. The processing of ICESat data involves four main steps: filtering of dh, classification of ICESat footprints, identification of on-glacier and off-glacier measurements, and correction of mean dh over glacier surface and linear trend fitting.

### *3.2. Glacier–Climate Relationship*

Long-term changes in local temperature and precipitation were analyzed using the CN05 grid dataset [35]. This gridded dataset, at a resolution of 0.5 × 0.5 degree, was constructed by interpolating climatic records of 2416 meteorological stations in China, with the "anomaly approach" which firstly interpolates climate variables with thin plate smoothing splines and then adds a gridded daily anomaly derived from angular distance weighting method [36]. A Digital elevation model (DEM) was used as a reference in the interpolation, and thus the dataset can represent climate over the mountainous regions. This dataset has been validated with good quality [37,38] and widely applied to analyze long-term climate change in China (e.g., [39]). We extracted monthly temperature and precipitation estimates over 1976–2013 from the grid where the glaciers are located. The estimates of precipitation (temperature) show similar intra-annual and inter-annual pattern to that recorded at the closest meteorological station Tuotuohe (the comparison is shown in Figure S4 in the supporting material). According to the hydrological year, the climate data were aggregated to the seasonal level: cold (winter) season (October to April), and warm (summer) season (May to September).

To examine glacier change with respect to large-scale atmospheric circulations, the following datasets were utilized: ERA (European Reanalysis) data including the monthly geopotential height/wind fields at the 500 hPa levels, the grid 2 m air temperature data from the European

Centre for Medium-range Weather Forecasts [40]. The principal component-based Hurrell NAO index, signifying the sea level pressure (SLP) anomalies over the Atlantic sector (20°N–80°N, 90°W–40°E) [41], is used to represent the strength of westerlies in this study. We also examined the indices of two major Asian monsoon systems: the Indian Monsoon index (IMI) which is the normalized anomalies of SLP difference between the Indian sea zone (40°E–80°E, 5°N–15°N) and central Asia (70°E–90°E, 20°N–30°N) [42], and the East Asian Summer Monsoon Index (EASMI) which is defined as an area-averaged dynamical normalized seasonality at 850 hPa within the domain (10°N–40°N, 110°E–140°E) [43]. The North Annular Mode (NAM) index, denoting SLP anomalies in the Northern Hemisphere (NH: 20°N–90°N), is an important index closely associated with large-scale atmospheric circulations such as NAO and westerlies. Whereas SLP anomalies over the north Pacific were examined with the North Pacific Index (NPI), the area-weighted SLP over the region 30°N–65°N, 160°E–140°W [44]. The El Niño and La Niña episodes can be represented by the Southern Oscillation Index (SOI) which is calculated as the normalized anomaly of mean SLP difference between Tahiti and Darwin. The negative (positive) SOI values coincide with warm (cold) ocean water across the eastern tropical Pacific in typical El Niño (La Niña) episodes. Annual, summer and winter NAO and SOI time series were used to evaluate the influences on time scales of yearly, warm season and cold season respectively. The summer monsoons are pronounced in warm seasons, therefore only summer season composites (JJA) were examined; while the NAM and NPI are pronounced in winter seasons, we only examined winter season composites.

Linear regression analysis was performed to estimate trends of glacier area, local temperature and precipitation changes. We examined possible relationships between local climatic variables (temperature and precipitation) and atmospheric circulation indices by calculating their correlation coefficients based on detrended time series data. The detrending was conducted by subtracting the trends estimated with the linear fitting method from the original climatic data and indices (difference detrending method), to mitigate spurious correlations due to potential common trends presented in the original time-series data. Spearman's rank correlation coefficient ($R$ in short) was used to examine the relationship between glacier area and climate variables. Unless otherwise stated, all p-values for the trends and correlation coefficients were evaluated at alpha = 0.05, and long-term (multi-year) averages refer to statistics over the period of 1976–2013.

## 4. Results and Discussion

### *4.1. The Change of Glacier Area and Surface Elevation*

The variation of glacier area during the period of 1976–2013 is shown in Figure 3. Overall, the glacier area observed in 1986 is far above the long-term average, which may be associated with mapping uncertainties due to the influence of persistent seasonal cover and will be discussed in details in Section 4.3. The 1986 observation is therefore excluded in the following statistics to reduce uncertainties. Overall, the average glacier area is 83.9 $\pm$ 3.6 km$^2$ ($n$ = 17, one standard deviation). The total glacier area significantly decreased at a linear rate of $-0.31 \pm 0.04$ km$^2$·year$^{-1}$, equivalent to a percentage changing rate of $-0.37\% \pm 0.05\%$ year$^{-1}$. According to this linear fit, the total glacier area lost during the study period is estimated to be 13.7% $\pm$ 1.85% year$^{-1}$. To explore more information about glacier area changes during the past 38 years, we calculated the mean glacier area in different periods (Period 1: 1988–1995; Period 2: 2000–2004; Period 3: 2007–2013) according to the cluster of samples (shown as multiplication marks in Figure 3a). The statistics outlines the changes of glacier shrinking rate (estimated as the slope of the line between neighboring multiplication marks in Figure 3a): $-0.11$ km$^2$·year$^{-1}$ from 1976 to Period 1, $-0.36$ km$^2$·year$^{-1}$ from Period 1 to Period 2, and $-0.40$ km$^2$·year$^{-1}$ from Period 2 to Period 3. This indicates that glacier shrinkage is particularly obvious since the late 1990s and the shrinkage slightly accelerated in the 2000s. However, there are few observations in some periods such as 1976–1986, which pose uncertainties for evaluating detailed glacier changes in the 1980s and the statistics of linear rates.

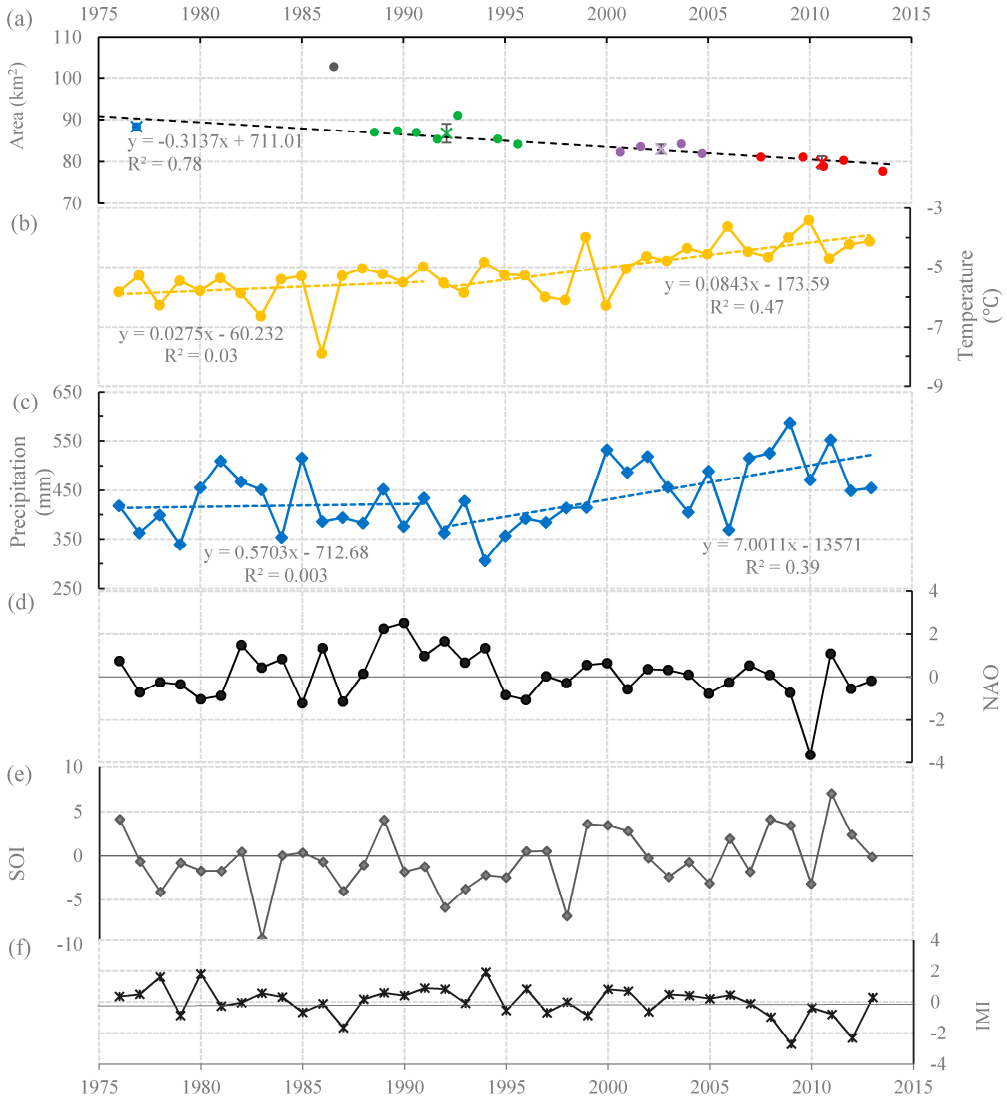


**Figure 3.** The variation of glacier area (**a**) in relation to annual mean temperature (**b**); annual total precipitation (**c**); North Atlantic Oscillation (NAO) (**d**); winter Southern Oscillation Index (SOI) (**e**); and Indian Monsoon Index (IMI) (**f**), during 1976–2013. The statistics is based on hydrological year (October to September). The linear trend in (**a**) is based on all observations excluding 1986, and the multiplication mark denotes average glacier area in different periods grouped by different colored dots, with the error bar showing the standard deviation of the mean value. For annual mean temperature and precipitation, linear trends are respectively shown for the two periods of 1976–1991 and 1992–2013.

The mean glacier surface elevation differences in Figure 4 (modified based on [34]) reveal a significant trend of glacier thinning at a linear rate 0.56 m·year$^{-1}$ ($p < 0.01$) over 2003–2008. Drastic lowering of glacier surfaces occurred in 2006. The standard deviations of the mean over-glacier dh, as shown in the error bar in Figure 4, vary in the range of 0.7 m to 1.9 m, which may partly reflect spatial variability in glacier thickness changes and the uncertainties associated with both the ICESat and SRTM data. For the off-glacier area, the elevation difference dh may be attributable to ICESat inter-campaign biases or bedrock uplift [5,45] and the trend is statistically insignificant. The ICESat-based glacier elevation trend, equivalent to a mass balance of −421.2 mm·year$^{-1}$ water equivalent (w.e.), is in good agreement with the mass balance (−487.2 mm·year$^{-1}$ w.e.) derived from glacier area changes in the period, which is analyzed in details in [34].

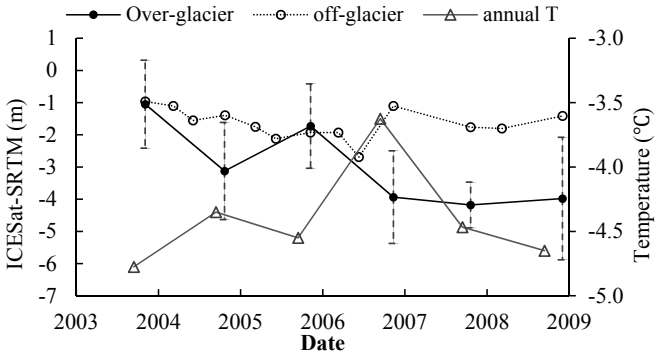


**Figure 4.** Variation of mean annual temperature, mean elevation differences between ICESat and SRTM over the glacier and off-glacier areas between 2003 and 2008 (modified based on [34]).

### *4.2. Long-Term Variation of Temperature and Precipitation*

The annual temperature increased at a linear rate of 0.53 °C per decade over 1976–2013 (Figure 3), much higher than the global warming trend of 0.15 °C~0.20 °C per decade that began in the late 1970s [46]. The increase of winter temperature (0.58 °C per decade) is more remarkable than that of summer temperature (0.45 °C per decade). The annual precipitation totals increased at a linear rate about 26 mm per decade. In terms of inter-decadal variations, the time-series climate data reveal significant increasing trends of temperature (0.95 °C per decade) and precipitation (62 mm per decade) during the latter 18 years (1995–2013), compared to the almost flat trends during the former 19 years (1976–1994) (Figure 3). Summer precipitation totals followed a similar variation to that of annual precipitation. Precipitation in winter fluctuated around an average level of 42.5 mm, except the year 1986 and 2000.

The time-series temperature and precipitation data in Figure 5 reveal two extreme climate events in 1986 and 2000. In the two years, winter precipitation reached extremely high amounts and correspondingly the mean temperature dropped to the lowest. We further examined the monthly precipitation time-series and found that the precipitation anomalies in the winter seasons of 1986/2000 mostly occurred in October 1985 and October 1999, respectively. In the two years, the precipitation anomaly in October accounts for over 70% of the seasonal anomaly. In particular, the extremely cold winter in 1986 has been documented as snow storm disaster that occurred in October-November 1985 in the central QTP [47].

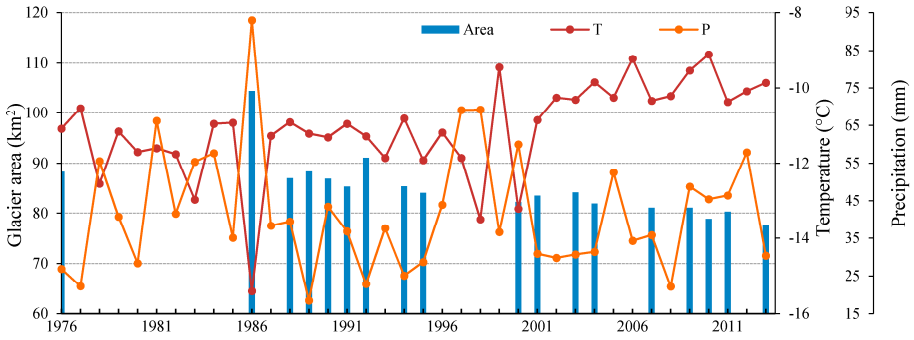


**Figure 5.** The variation in mean temperature (T) and total precipitation (P) in the winter season in relation to glacier area changes.

### *4.3. Relationship between Glacier Variation and Local Climate Variables*

Given the extreme local climate conditions in 1986 and 2000, the statistics on the correlation coefficients between glacier area and climate variables (Table 2) were divided into two groups: group

I based on all 18 samples and group II based on the 16 normal cases. In the two groups, the annual mean temperature shows the most significant relationship with glacier area ($R > 0.75$, $p < 0.01$). The winter temperature seems to be slightly more dominant than the summer temperature in normal years. The significant area-temperature relationship indicates that the annual temperature impact strongly on overall glacier advance/retreat s in the study area. Based on the 16 normal cases, the linear relationship between the glacier area and the annual temperature indicates an increase of 1 °C in annual temperature can contribute to loss of 5.1 $km^2$ in glacier area at a high confidence level ($p < 0.01$). The negative area-precipitation relationship is somehow unexpected, as normally precipitation contributes to glacier accumulation, e.g., by providing fresh snow. A possible explanation is that the effect of temperature increasing on melting overpowered the contribution of precipitation and therefore dominates the glacier mass balances. However, compared to the drastic recession of glaciers at a rate of over $-1.0$ m·$year^{-1}$ in the southern and southeastern QTP due to rising temperature coupled with decreasing precipitation [48,49], the high level of precipitation in this area may have slowed down the rate of glacier mass loss during the recent decade. Overall, in light of the dependence of glaciers on annual temperature, glaciers over the DKMD region will keep experiencing severe retreat if the warming trend continues.

**Table 2.** Correlation between glacier area and climate variables. Group I is statistics based on all area samples and group II is based on those excluding two extreme climate years. Results in bold are significant at the 0.01 level and those in italics at 0.05.

| Climate Parameters and Season | Group I: All Cases ($n$ = 18) | | Group II: Normal Cases (Excluding 1986, 2000) | |
|---|---|---|---|---|
| | Correlation Coefficient | $p$-Value | Correlation Coefficient | $p$-Value |
| Temperature | | | | |
| -Annual | **−0.78** | 0.00 | **−0.85** | 0.00 |
| -Summer | **−0.75** | 0.00 | **−0.72** | 0.00 |
| -Winter | **−0.71** | 0.00 | **−0.76** | 0.00 |
| Precipitation | | | | |
| -Annual | **−0.65** | 0.00 | **−0.64** | 0.01 |
| -Summer | **−0.61** | 0.01 | *−0.53* | 0.04 |
| -Winter | −0.34 | 0.17 | *−0.57* | 0.02 |
| North Atlantic Oscillation | | | | |
| -Annual | **0.67** | 0.00 | **0.65** | 0.01 |
| -Summer | *0.49* | 0.04 | 0.48 | 0.06 |
| -Winter | **0.57** | 0.01 | **0.74** | 0.00 |
| Southern Oscillation Index | | | | |
| -Annual | −0.45 | 0.06 | −0.38 | 0.15 |
| -Summer | −0.34 | 0.17 | −0.32 | 0.24 |
| -Winter | −0.09 | 0.71 | −0.11 | 0.68 |
| North Annular Mode | *−0.47* | 0.05 | **−0.69** | 0.00 |
| North Pacific Index | −0.20 | 0.43 | −0.05 | 0.86 |
| Indian Monsoon Index | 0.44 | 0.07 | *0.59* | 0.02 |
| East Asian Summer Monsoon Index | 0.20 | 0.44 | 0.17 | 0.54 |

A close look at the glacier changes in the recent decade further confirms the role of temperature in determining glacier changes. As shown in Figure 4, the mean glacier surface elevation was closely connected with the variation of annual temperature. The glaciers showed noticeable lowering as the annual temperature increased in 2004 and 2006. The strong thinning in 2006 was accompanied by significant increase in annual temperature (0.9 °C) and decrease of summer precipitation by 20%.

In 1986 and 2000, the observed glacier area deviates from the fitted area-temperature relationship based on normal cases. The situation may be caused by several factors. Firstly, the mapping uncertainty due to inclusion of peripheral snow cover can be large in 1986, in particular, as there was plenty snow cover in the winter season which might have sustained through the melting season. The far

above-average glacier area in 1986 is probably problematic from the perspective of glaciological process; the observation, however, offers potential lights into glacier accumulation/advance, given it is the only high-quality image available for that period. Although it is difficult to quantify the real glacier advance in 1986 because of lacking observations prior to 1986, the snow storm events in 1986 (specifically in October–November 1985) may contribute to significant glacier advance, whereas the magnitude of increment may not be as large as that indicated in the current observations. The potential impact of such events on glacier mass balance is at least two-fold: (1) contributing to ice accumulation by providing considerable fresh snow; and (2) slowing down snow melting because of reduced solar radiation and temperature due to increase in surface albedo. The second point can be supported by the fact that the mean temperature during October 1985 and April 1986 was rather low (Figure 4). Compared to the 1985 case, the glacier area in 2000 in a similar climate condition did not behave the same as that in 1986. The possible explanations besides mapping uncertainties may lie in three aspects. First, the winter precipitation total in 2000 is not as high as that in 1986. Second, the high temperature in 2000 summer (0.8 °C more than that in 1986) may have significantly accelerated the glacier melting. Third, the glaciers experienced significant shrinkage between 1986 and 2000, which may have resulted in the disappearance of small glaciers. The third point is critical, as small-size glaciers probably play a dominating role in contributing to the observed glacier area changes due to their high sensitivity to climate change and the short response time. However, it is not clear about the response time of multiple glaciers with different lengths, thickness and hypsometry in the study region. Given the glaciers are of semi-maritime type and the variability in glacier area, the mean response time could be within a few years.

### *4.4. Links between Glacier Variation and Macroscale Atmospheric Circulations*

The total glacier area shows significant correlations with NAO, NAM and IMI (Table 2). The variation of glacier area was positively associated with the status of NAO, particularly winter NAO ($p < 0.01$). The relatively large glacier area (e.g., in 1976, 1989 and 1992) was associated with the strong positive phase of NAO, while the intermediate or negative phase of NAO coincided well with the retreating trend of glaciers after 2000 (Figure 3). The IM also shows a weakening trend since 1990, which probably explains the positive IMI-glacier relationship. When considering the 1986 and 2000 cases, the correlation coefficients between glacier area and NAO and NAM decreased but the relationships remain significant; whereas the correlation with IMI does not reach the significant level (Table 2).

The relationships between local climate variables and macroscale climate index provide a clue on how atmospheric circulations impact on the glaciers. As shown in Table 3, the variation of local climate variables show close associations with different large-scale atmospheric circulations, the most significant being NAO and SOI. In winter, the mean temperature produces significant negative relationship with NAO and positive relationship with SOI, and the amount of precipitation shows no significant correlation with other climate variables; whereas in summer, the mean temperature and the amount of precipitation both show close connection with NAO (annual NAO and summer NAO, respectively). The negative correlations between the summer/winter temperature and annual/winter NAO suggest that summer/winter temperatures tend to be higher (lower) over the central QTP when the NAO is more negative (positive), whereas in summer when most of the precipitation falls, the more negative (positive) phase of NAO may indicate wetting (drying) climate than normal. Figure 3 shows that since the middle 1990s, NAO has been in a relatively low phase, which couples well with the increasing temperature and precipitation over the DKMD region. This suggests that the negative relationships between NAO and local temperature/precipitation keep on the inter-decal time-scale. Note that there are no significant relationships between the local summer precipitation, IMI and EASMI, suggesting that summer precipitation has no direct links with the monsoon systems.

**Table 3.** Correlation matrix of relationships between climate variables after de-trending the original time series data. The statistics is based on 36-year samples over 1976–2013 (excluding abnormal years of 1986 and 2000). Numbers in bold denote significance at the 0.01 level and those in italics at 0.05. The full form of some climate variables: North Annual Mode (NAM), North Pacific Index (NPI), Indian Monsoon Index (IMI), and East Asian Summer Monsoon Index (EASMI).

| | **Temperature** | | | **Precipitation** | | | **NAO** | | | **SOI** | | | **NAM** | **NPI** | **IM** | **EASMI** |
|---|---|---|---|---|---|---|---|---|---|---|---|---|---|---|---|---|
| | **Ann.** | **Sum.** | **Win.** | **Ann.** | **Sum.** | **Win.** | **Ann.** | **Sum.** | **Win.** | **Ann.** | **Sum.** | **Win.** | | | | |
| Temperature | | | | | | | | | | | | | | | | |
| -Ann. | 1.00 | | | | | | | | | | | | | | | |
| -Sum. | **0.48** | 1.00 | | | | | | | | | | | | | | |
| -Win. | **0.93** | 0.21 | 1.00 | | | | | | | | | | | | | |
| Precipitation | | | | | | | | | | | | | | | | |
| -Ann. | −0.07 | −0.17 | −0.04 | 1.00 | | | | | | | | | | | | |
| -Sum. | 0.01 | −0.21 | 0.06 | **0.97** | 1.00 | | | | | | | | | | | |
| -Win. | −0.19 | 0.13 | −0.28 | 0.04 | −0.14 | 1.00 | | | | | | | | | | |
| North Atlantic Oscillation | | | | | | | | | | | | | | | | |
| -Ann. | −0.24 | *−0.34* | −0.15 | −0.09 | −0.06 | −0.22 | 1.00 | | | | | | | | | |
| -Sum. | 0.17 | 0.19 | 0.11 | *−0.40* | *−0.38* | −0.14 | 0.23 | 1.00 | | | | | | | | |
| -Win. | −0.32 | −0.18 | *−0.34* | −0.06 | −0.02 | −0.10 | **0.60** | 0.15 | 1.00 | | | | | | | |
| Southern Oscillation Index | | | | | | | | | | | | | | | | |
| -Ann. | *0.32* | −0.04 | *0.33* | 0.23 | 0.27 | −0.10 | −0.06 | −0.01 | −0.19 | 1.00 | | | | | | |
| -Sum. | 0.01 | 0.27 | −0.09 | 0.12 | 0.10 | 0.23 | −0.21 | 0.11 | −0.17 | **0.45** | 1.00 | | | | | |
| -Win. | 0.27 | −0.21 | *0.35* | 0.25 | 0.28 | −0.18 | 0.11 | −0.07 | −0.09 | **0.85** | −0.03 | 1.00 | | | | |
| NAM | *0.36* | 0.26 | *0.34* | −0.02 | −0.07 | 0.16 | **−0.66** | −0.08 | **−0.95** | 0.20 | 0.23 | 0.06 | 1.00 | | | |
| NPI | 0.30 | 0.06 | 0.25 | 0.09 | 0.13 | −0.21 | *0.35* | 0.06 | 0.16 | **0.46** | −0.17 | **0.56** | −0.23 | 1.00 | | |
| IMI | −0.17 | 0.02 | −0.15 | −0.20 | −0.19 | −0.27 | 0.18 | *0.37* | −0.12 | −0.24 | 0.05 | −0.31 | 0.15 | −0.18 | 1.00 | |
| EASMI | 0.21 | −0.10 | 0.24 | −0.10 | −0.10 | 0.18 | 0.18 | 0.09 | 0.14 | 0.05 | **−0.45** | 0.32 | −0.15 | 0.31 | −0.22 | 1.00 |

NAO and SOI are found to be widely related to other climate variables. Winter NAO is closely correlated with NAM ($R = -0.95$, $p < 0.01$), and summer NAO is positively correlated with IMI ($R = 0.37$, $p < 0.05$). The positive IMI-NAO relationship confirms that the intensity of IM is more impacted by oscillation over the Atlantic, rather than Pacific, over recent decades [50,51]. The status of SOI is closely linked with NPI, especially in winter seasons. The significant inverse EASMI-SOI relationship supports an enhanced link between the intensity of East Asia summer monsoon and oscillation over the Pacific, which agrees with previous research [52].

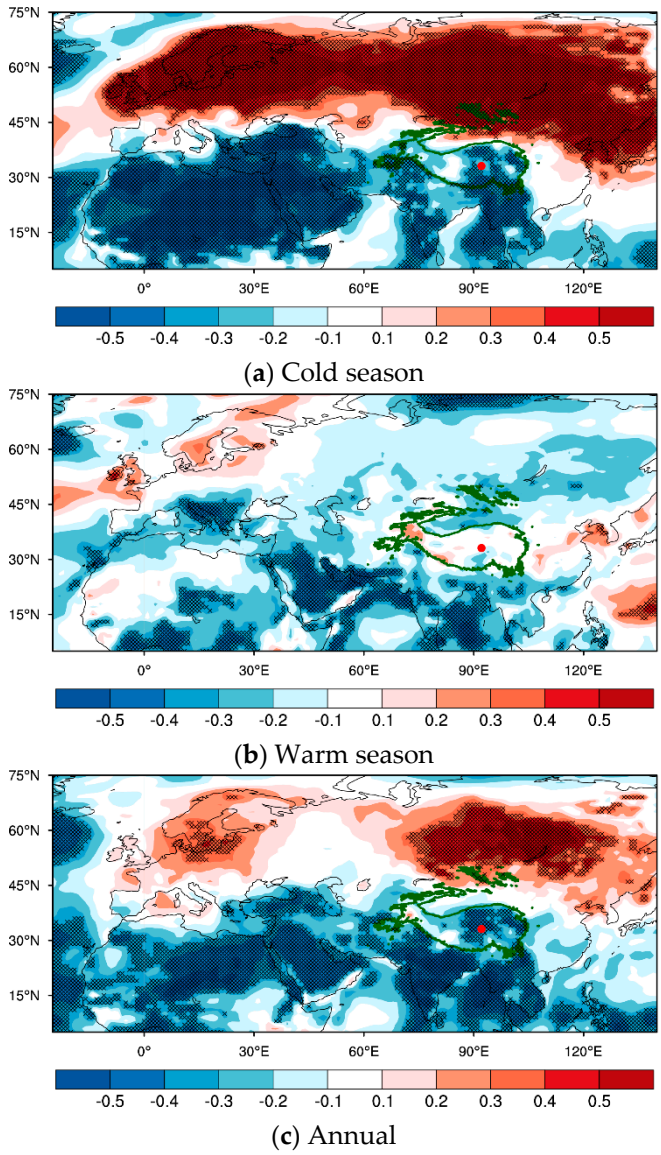


**Figure 6.** Correlation coefficients between NAO and 2 m air temperature on time scales of: cold season (**a**); warm season (**b**); and annual (**c**), based on ERA reanalysis data (1976–2013). The black cross filling denotes significance at a confidence level of 95%, and the red dots represent the location of the study region.

The relationship between NAO and temperature over the DKMD can be confirmed based on spatially continuous re-analysis data. Figure 6 shows the correlation coefficients between mean NAO and 2 m air temperature in the winter season, summer season and annual. It is clear that NAO has wide connections with temperature variations over the NH, particularly in the winter season. On the time scale of annual mean, NAO is positively connected with temperature in the northern Europe and

Russia, and is negatively correlated with air temperature over the lands of the Arab, India, and the central QTP. The connections between NAO and temperature over the European and Russian regions have been confirmed in previous research [53,54]. Over our study region, the NAO-temperature relationship is weak in the summer season but significant in the winter season, which agrees well with the statistics in Table 3. To further investigate how NAO influences local climate over the study region, we examined the difference of geopotential height/wind fields at the 500 hPa levels between low NAO and high NAO phases in winter seasons and summer seasons respectively, as shown in Figure 7. The criterion for selecting the specific high/low NAO years is that NAO is at least one standard deviation above/below the multi-year average. The specific years selected is given in Table 4. When NAO is more negative, the 500 hPa geopotential height in the western and central Europe and northeastern Eurasia is considerably decreased, while it is significantly higher in northern Europe, central Eurasia and southern QTP regions (Figure 7a). The changes of potential height, combined with the pattern of wind vector anomalies, shape two strong cyclonic circulations in Eastern Europe and northeastern Eurasia. In particular, the latter represents a weakened Siberian High (centered on Lake Baikal) and strengthened westerly winds between 30°N and 45°N of Asia. According to [55], strong westerlies can decrease the incursions of colder air from the north to the south. The weakened Siberian High and strengthened westerlies may explain why winter temperatures over central QTP are lower in years with more negative NAO. In summer seasons, when NAO is more negative, the 500 hPa geopotential height considerably increases over the mid-latitude Eurasia (between 30°N and 45°N), which extends from southern Europe to northeastern Eurasia; whereas it decreases over northern Europe, central QTP and northeastern China (Figure 7b). The changes of the geopotential height and the pattern of wind anomalies are characterized by cyclonic circulations over inner QTP which favor local precipitation production. Besides, the stronger southwesterly winds (Figure 7d) along the southern edges of the plateau indicate enhanced moisture advection from the Mediterranean Sea toward the QTP. These factors probably explain why there is more precipitation in years with more negative NAO in the summer season.

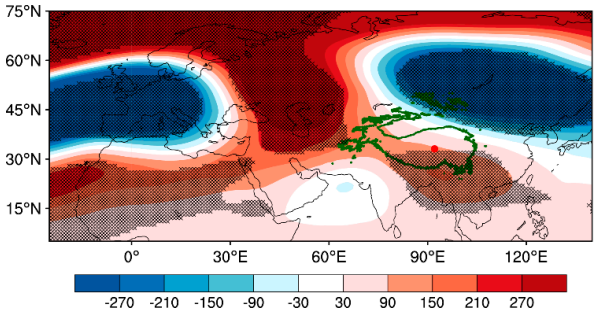


(**a**) Cold season: difference in geopotential height

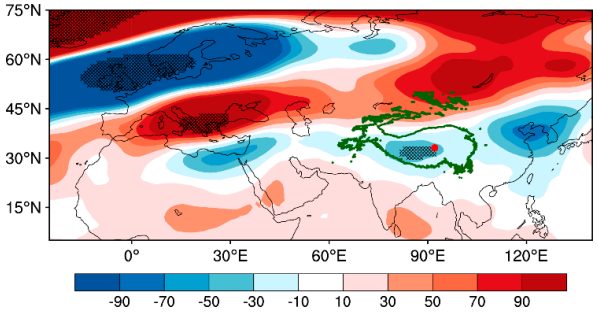


(**b**) Warm season: difference in geopotential height

**Figure 7.** *Cont*.

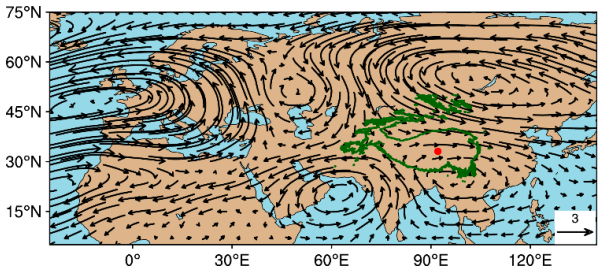


(**c**) Cold season: difference in wind speed field

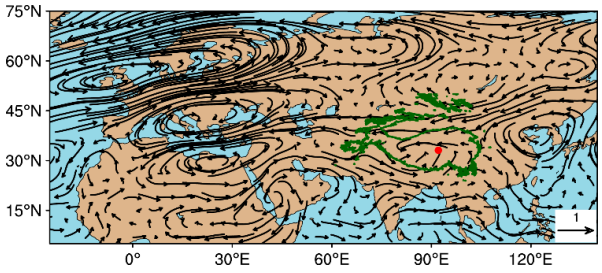


(**d**) Warm season: difference in wind speed field

**Figure 7.** Composite differences in the mean 500 hPa geopotential height (the upper row) and wind speed field (the lower row) in the: cold season (**a**,**c**); and warm season (**b**,**d**) between the group of years with low NAO and high NAO. Refer to Table 4 for specific years selected. The black cross filling in (**a**,**b**) denotes significance at a confidence level of 95%, and the ret dots represent the location of the study region.

**Table 4.** Selected groups of low NAO and high NAO years in the warm and cold season for the construction of composite charts.

| Season | Low NAO Years | High NAO Years |
|---|---|---|
| Cold season | 1996, 2001, 2006, 2010, 2013 | 1989, 1990, 1992, 1993, 2000, 2012 |
| Warm season | 1987, 1993, 2007, 2008, 2009, 2011, 2012 | 1983, 1989, 1994, 1996, 2013 |

In summary, the state of NAO plays an important role in driving the climate variability and glacier changes over the DKMD region in central QTP. The negative (positive) phase of NAO favor warm (cold) winters and high (low) annual temperature through modulating the intensity of the Siberian High and westerlies in the mid-latitude Eastern Asia, resulting in glacier recession (gain). Despite the fact that the low phase of NAO in the summer season contributes to increasing precipitation in the study region, the rise of temperature overpowered the effect of precipitation and governed the glacier changes.

### *4.5. The Role of SOI in Climate Variability*

SOI represents oscillations over the Pacific which have wide influences on climate variability in the NH. We also found a positive relationship between SOI and winter temperature over the study region. Many studies suggested that SOI can impact the QTP region through the link of IM or EASM [20–22,56]. However, it is obvious that the summer monsoon systems have no direct impact on the mid-latitude central QTP over recent decades. Furthermore, previous studies have confirmed that the ENSO-IM relationship has weakened since the late 1970s.

The SOI, however, might be relevant to the abnormal snow storm events in the central plateau. Although none of the climatic indices in this study has been identified to be responsible for the anomalous snow storms in October of 1985 and 1999, the super ENSO events (associated with strong negative phased of SOI) that occurred in 1983 and 1998 might have played a role. Previous

research suggests that SOI affects snow depth over central QTP with a lag time of one or two years [57]. Regarding the cases on 1985 and 1999, the specific process is however not certain. If such tele-connection exists, the ENSO events may contribute to glacier mass gain in the central plateau by bringing high precipitation. The physical mechanism linking SOI and climate variation over central QTP is yet unclear, and this requires further research.

The relationship between local climate variables and NAO, SOI, however, may have varied in a long time frame [20], and the relationships between local climate and NAO, SOI are not always linear. Fluctuations in these atmospheric circulations may not fully explain the variability of glacier changes, and there may be other climate forcings affecting the variation of glaciers over the QTP. Further research is needed to investigate which and how regional atmospheric circulations affect the climate variability and glacier changes in different regions of the QTP.

## 5. Summary and Conclusions

The increasing availability of remote sensing data enables detailed investigation of regional glacier changes and the response to climate change. This study presents areal and thickness changes of glaciers in the DKMD region in central QTP based on sequential Landsat images and ICESat elevation data, and explores the causal explanation of the changes from the perspective of local and macroscale climate background. The results show that the examined glaciers experienced notable shrinkage over recent decades, with the total area decreasing at a linear rate of $0.37\% \pm 0.05\%$ year$^{-1}$ during the period of 1976–2013. Glacier shrinkage has been particularly distinct since the late 1990s and slightly accelerated in the 2000s. During 2003 and 2008, the mean glacier elevations lowered at a linear rate of 0.56 m·year$^{-1}$. Interpretation of the glacier area and elevation changes with regard to climate change reveals the dominant role of increasing temperature, particularly in the winter season and since the middle 1990s. The precipitation variations are characterized by a significant rising trend since the 1990s. The high level of precipitation in the 21st century might have alleviated glacier recession compared to the warm-dry southern QTP regions. In particular, the cold and snowy winters of 1986 and 2000 due to severe snow storm events over central QTP, may have a significant contribution to glacier advance or restrained retreat in the following years due to combined effect of increased fresh snow and surface albedo, and reduced temperature. However, the current glacier area observation for 1986 is prone to large uncertainties associated with persistent seasonal snow cover, and more evidence is required to quantify the impact of extremely snow events on the glacier mass balances.

With respect to macroscale atmospheric circulations, our analysis suggests that the glacier variation over the DKMD region during 1976–2013 were impacted by oscillation in the North Atlantic Ocean. The state of NAO drives local climate variability through modulating the strength of Siberian High and westerlies over the mid-latitude Eurasia. The negative (positive) phase of NAO is associated with a weaker (stronger) Siberian Anticyclone and stronger (weaker) westerlies, resulting in warm (cold) winters and high (low) annual and glacier recession (advance). The Super ENSO events in 1983/1998 seem to be associated with the two snow storm events occurring in 1985/1999, but the mechanism is unclear. There is no strong evidence supporting the principal role of the monsoon systems (IM and EASM) in driving climate variabilities and glacier changes over the study region. Further research is needed to investigate the physical processes linking climate variability and large-scale atmospheric circulations, and the causes and impacts of extreme climate events over the plateau.

**Supplementary Materials:** The following are available online at www.mdpi.com/2072-4292/9/2/114/s1, Figure S1: Glacier outlines (red or yellow lines) mapped from Landsat MSS/TM/ETM+/OLI images, Figure S2: Mapping results based on MSS image acquired on 11 November 1976, Figure S3: Glacier mapping in three years (column 1, 2001; column 2, 2003, column 3, 2010) with reference to clear images (row 2) over the cloud-covered parts, Figure S4: Multi-year averaged (1976-2011) monthly temperature (lines) and precipitation (bars) over the DKMD and Tuotuohe based on CN05 gridded climate dataset in comparison with records derived from the Tuotuohe meteorological station, Figure S5: Inter-annual variation of precipitation (a) and temperature (b) over 1976-2011 for the DKMD region (CN05 gridded dataset), Tuotuohe (CN05 gridded dataset) in comparison with those recorded at the Tuotuohe meteorological station.

**Acknowledgments:** The meteorological data (CN05 grid data and station records) were provided by China Meteorological Data Sharing Service System (CMDSSS). ICESat data were derived from the National Snow and Ice Data Center (NSIDC). Atmospheric indices including NAO, NAM, NPI and SOI were obtained from Climate Analysis Section, National Center for Atmospheric Research (NCAR). Monsoon Indices IMI and EASMI were respectively downloaded from Asia-Pacific Data-Research Center and Li's page. This study was supported by a Ph.D. studentship offered by the Hong Kong Polytechnic University, a Research Grant Council of the Hong Kong Special Administrative Region (Project No.: PolyU 5147/13E), and a Public Welfare Research Fund from the National Administration of Surveying, Mapping and Geoinformation. We sincerely appreciate constructive comments and suggestions from the guest editors and three anonymous reviewers.

**Author Contributions:** Linghong Ke and Xiaoli Ding designed the study. Linghong Ke processed the satellite data (Landsat, ICESat and CN05) and wrote the manuscript. Wenkai Li processed the ERA re-analysis data and figures. Wenkai Li and Bo Qiu helped in the analysis of atmospheric circulations. Xiaoli Ding edited and commented on the manuscript.

**Conflicts of Interest:** The authors declare no conflict of interest.

## Abbreviations

The following abbreviations are used in this manuscript:

| | |
|---|---|
| CGI | China Glacier Inventory |
| DEM | Digital Elevation Model |
| DKMD | Dongkemadi (place name) |
| EASM | East Asian Summer Monsoon |
| EASMI | East Asian Summer Monsoon Index |
| ENSO | El Niño Southern Oscillation |
| ERA | European Reanalysis |
| IM | Indian Monsoon |
| IMI | Indian Monsoon Index |
| NAM | North Annular Mode |
| NAO | North Atlantic Oscillation |
| NH | Northern Hemisphere |
| NPI | North Pacific Index |
| QTP | Qinghai-Tibet Plateau |
| SLP | Sea level pressure |
| SOI | Southern Oscillation Index |

## References

1. Immerzeel, W.W.; van Beek, L.P.H.; Bierkens, M.F.P. Climate change will affect the Asian water towers. *Science* **2010**, *328*, 1382–1385. [CrossRef]
2. Yao, T.; Thompson, L.; Yang, W.; Yu, W.; Gao, Y.; Guo, X.; Yang, X.; Duan, K.; Zhao, H.; Xu, B.; et al. Different glacier status with atmospheric circulations in Tibetan Plateau and surroundings. *Nat. Clim. Chang.* **2012**, *2*, 663–667. [CrossRef]
3. Song, C.; Sheng, Y. Contrasting evolution patterns between glacier-fed and non-glacier-fed lakes in the Tanggula Mountains and climate cause analysis. *Clim. Chang.* **2016**, *135*, 493–507. [CrossRef]
4. Liu, S.; Sun, W.; Shen, Y.; Li, G. Glacier changes since the Little Ice Age maximum in the western Qilian Shan, northwest China, and consequences of glacier runoff for water supply. *J. Glaciol.* **2003**, *49*, 117–124.
5. Kääb, A.; Berthier, E.; Nuth, C.; Gardelle, J.; Arnaud, Y. Contrasting patterns of early twenty-first-century glacier mass change in the Himalayas. *Nature* **2012**, *488*, 7412–7498. [CrossRef] [PubMed]
6. Gardner, A.S.; Moholdt, G.; Cogley, J.G.; Wouters, B.; Arendt, A.A.; Wahr, J.; Berthier, E.; Hock, R.; Pfeffer, W.T.; Kaser, G.; et al. A reconciled estimate of glacier contributions to sea level rise: 2003 to 2009. *Science* **2013**, *340*, 852–857. [CrossRef] [PubMed]
7. Ke, L.; Ding, X.; Song, C. Heterogeneous changes of glaciers over the western Kunlun Mountains based on ICESat and Landsat-8 derived glacier inventory. *Remote Sens. Environ.* **2015**, *168*, 13–23. [CrossRef]
8. Ye, Q.; Bolch, T.; Naruse, R.; Wang, Y.; Zong, J.; Wang, Z.; Zhao, R.; Yang, D.; Kang, S. Glacier mass changes in Rongbuk catchment on Mt. Qomolangma from 1974 to 2006 based on topographic maps and ALOS PRISM data. *J. Hydrol.* **2015**, *530*, 273–280. [CrossRef]

9. Yang, W.; Yao, T.; Guo, X.; Zhu, M.; Li, S.; Kattel, D.B. Mass balance of a maritime glacier on the southeast Tibetan Plateau and its climatic sensitivity. *J. Geophys. Res. Atmos.* **2013**, *118*, 9579–9594. [CrossRef]
10. Tian, L.; Yao, T.; MacClune, K.; White, J.W.C.; Schilla, A.; Vaughn, B.; Vachon, R.; Ichiyanagi, K. Stable isotopic variations in west China: A consideration of moisture sources. *J. Geophys. Res. Atmos.* **2007**, *112*. [CrossRef]
11. Koji, F.; Ageta, Y.; Pu, J.; Yao, T. Mass balance of Xiao Dongkemadi glacier on the central Tibetan Plateau from 1989 to 1995. *Ann. Glaciol.* **2000**, *31*, 159–163.
12. Paul, F.; Barrand, N.; Baumann, S.; Berthier, E.; Bolch, T.; Casey, K.; Frey, H.; Joshi, S.; Konovalov, V.; Bris, R.L. On the accuracy of glacier outlines derived from remote-sensing data. *Ann. Glaciol.* **2013**, *54*, 171–182. [CrossRef]
13. Redpath, T.; Sirguey, P.; Fitzsimons, S.; Kääb, A. Accuracy assessment for mapping glacier flow velocity and detecting flow dynamics from ASTER satellite imagery: Tasman Glacier, New Zealand. *Remote Sens. Environ.* **2013**, *133*, 90–101. [CrossRef]
14. Bamber, J.L.; Rivera, A. A review of remote sensing methods for glacier mass balance determination. *Glob. Planet. Chang.* **2007**, *59*, 138–148. [CrossRef]
15. Racoviteanu, E.A.; Williams, W.M.; Barry, G.R. Optical Remote Sensing of Glacier Characteristics: A Review with Focus on the Himalaya. *Sensors* **2008**, *8*, 3355–3383. [CrossRef] [PubMed]
16. Neckel, N.; Kropácek, J.; Bolch, T.; Hochschild, V. Glacier mass changes on the Tibetan Plateau 2003–2009 derived from ICESat laser altimetry measurements. *Environ. Res. Lett.* **2014**, *9*, 014009. [CrossRef]
17. Francis, J.A.; Vavrus, S.J. Evidence linking Arctic amplification to extreme weather in mid-latitudes. *Geophys. Res. Lett.* **2012**, *39*. [CrossRef]
18. Screen, J.A.; Simmonds, I. Exploring links between Arctic amplification and mid-latitude weather. *Geophys. Res. Lett.* **2013**, *40*, 959–964. [CrossRef]
19. Mölg, T.; Maussion, F.; Scherer, D. Mid-latitude westerlies as a driver of glacier variability in monsoonal High Asia. *Nat. Clim. Chang.* **2013**, *4*, 68–73. [CrossRef]
20. Wang, N.L.; Thompson, L.G.; Davis, M.E.; Mosley-Thompson, E.; Yao, T.D.; Pu, J.C. Influence of variations in NAO and SO on air temperature over the northern Tibetan Plateau as recorded by $\delta^{18}O$ in the Malan ice core. *Geophys. Res. Lett.* **2003**, *30*, 2167. [CrossRef]
21. Xu, H.; Hong, Y.T.; Hong, B.; Zhu, Y.X.; Wang, Y. Influence of ENSO on multi-annual temperature variations at Hongyuan, NE Qinghai-Tibet plateau: Evidence from $\delta^{13}C$ of spruce tree rings. *Int. J. Climatol.* **2010**, *30*, 120–126. [CrossRef]
22. Xu, G.; Chen, T.; Liu, X.; Jin, L.; An, W.; Wang, W. Summer temperature variations recorded in tree-ring $\delta^{13}C$ values on the northeastern Tibetan Plateau. *Theor. Appl. Climatol.* **2011**, *105*, 51–63. [CrossRef]
23. Zhao, H.; Xu, B.; Yao, T.; Wu, G.; Lin, S.; Gao, J.; Wang, M. Deuterium excess record in a southern Tibetan ice core and its potential climatic implications. *Clim. Dyn.* **2012**, *38*, 1791–1803. [CrossRef]
24. Guo, W.; Liu, S.; Xu, J.; Wu, L.; Shangguan, D.; Yao, X.; Wei, J.; Bao, W.; Yu, P.; Liu, Q. The second Chinese glacier inventory: Data, methods and results. *J. Glaciol.* **2015**, *61*, 357–372. [CrossRef]
25. Chen, F.-H.; Chen, J.-H.; Holmes, J.; Boomer, I.; Austin, P.; Gates, J.B.; Wang, N.-L.; Brooks, S.J.; Zhang, J.-W. Moisture changes over the last millennium in arid central Asia: A review, synthesis and comparison with monsoon region. *Quat. Sci. Rev.* **2010**, *29*, 1055–1068. [CrossRef]
26. Li, W.; Guo, W.; Hsu, P.-C.; Xue, Y. Influence of the Madden–Julian oscillation on Tibetan Plateau snow cover at the intraseasonal time-scale. *Sci. Rep.* **2016**, *6*. [CrossRef] [PubMed]
27. Pu, J.; Yao, T.; Yang, M.; Tian, L.; Wang, N.; Ageta, Y.; Koji, F. Rapid decrease of mass balance observed in the Xiao (Lesser) Dongkemadi Glacier, in the central Tibetan Plateau. *Hydrol. Process.* **2008**, *22*, 2953–2958. [CrossRef]
28. Hall, D.K.; Riggs, G.A.; Salomonson, V.V. Development of methods for mapping global snow cover using moderate resolution imaging spectroradiometer data. *Remote Sens. Environ.* **1995**, *54*, 127–140. [CrossRef]
29. Memarsadeghi, N.; Mount, D.M.; Netanyahu, N.S.; Le Moigne, J. A fast implementation of the ISODATA clustering algorithm. *Int. J. Comput. Geom. Appl.* **2007**, *17*, 71–103. [CrossRef]
30. Paul, F.; Bolch, T.; Kääb, A.; Nagler, T.; Nuth, C.; Scharrer, K.; Shepherd, A.; Strozzi, T.; Ticconi, F.; Bhambri, R.; et al. The glaciers climate change initiative: Methods for creating glacier area, elevation change and velocity products. *Remote Sens. Environ.* **2015**, *162*, 408–426. [CrossRef]

31. Paul, F.; Kaab, A.; Maisch, M.; Kellenberger, T.; Haeberli, W. The new remote-sensing-derived Swiss glacier inventory: I. Methods. *Ann. Glaciol.* **2002**, *34*, 355–361. [CrossRef]
32. Pieczonka, T.; Bolch, T. Region-wide glacier mass budgets and area changes for the Central Tien Shan between ~1975 and 1999 using Hexagon KH-9 imagery. *Glob. Planet. Chang.* **2015**, *128*, 1–13. [CrossRef]
33. Zwally, H.J.; Schutz, B.; Abdalati, W.; Abshire, J.; Bentley, C.; Brenner, A.; Bufton, J.; Dezio, J.; Hancock, D.; Harding, D.; et al. ICESat's laser measurements of polar ice, atmosphere, ocean, and land. *J. Geodyn.* **2002**, *34*, 405–445. [CrossRef]
34. Ke, L.; Ding, X.; Song, C. Estimation of mass balance of Dongkemadi glaciers with multiple methods based on multi-mission satellite data. *Quat. Int.* **2015**, *371*, 58–66. [CrossRef]
35. Wu, J.; Gao, X. A gridded daily observation dataset over China region and comparison with the other datasets. *Chin. J. Geophys.* **2013**, *56*, 1102–1111.
36. New, M.; Hulme, M.; Jones, P. Representing twentieth-century space-time climate variability. Part II: Development of 1901–1996 monthly grids of terrestrial surface climate. *J. Clim.* **2000**, *13*, 2217–2238. [CrossRef]
37. You, Q.; Min, J.; Zhang, W.; Pepin, N.; Kang, S. Comparison of multiple datasets with gridded precipitation observations over the Tibetan Plateau. *Clim. Dyn* **2015**, *45*, 791–806. [CrossRef]
38. Shen, Y.; Xiong, A. Validation and comparison of a new gauge-based precipitation analysis over mainland China. *Int. J. Climatol.* **2016**, *36*, 252–265. [CrossRef]
39. Zhou, B.; Xu, Y.; Wu, J.; Dong, S.; Shi, Y. Changes in temperature and precipitation extreme indices over China: Analysis of a high-resolution grid dataset. *Int. J. Climatol.* **2015**. [CrossRef]
40. Dee, D.; Uppala, S.; Simmons, A.; Berrisford, P.; Poli, P.; Kobayashi, S.; Andrae, U.; Balmaseda, M.; Balsamo, G.; Bauer, P. The ERA-Interim reanalysis: Configuration and performance of the data assimilation system. *Q. J. R. Meteorol. Soc.* **2011**, *137*, 553–597. [CrossRef]
41. Hurrell, J.W. Decadal trends in the North Atlantic Oscillation: Regional temperatures and precipitation. *Science* **1995**, *269*, 676–679. [CrossRef] [PubMed]
42. Wang, B.; Wu, R.; Lau, K.M. Interannual variability of the Asian summer monsoon: Contrasts between the Indian and the Western North Pacific-East Asian Monsoons*. *J. Clim.* **2001**, *14*, 4073–4090. [CrossRef]
43. Li, J.; Zeng, Q. A unified monsoon index. *Geophys. Res. Lett.* **2002**, *29*, 1274. [CrossRef]
44. Trenberth, K.E.; Hurrell, J.W. Decadal atmosphere-ocean variations in the Pacific. *Clim. Dyn.* **1994**, *9*, 303–319. [CrossRef]
45. Siegfried, M.R.; Hawley, R.L.; Burkhart, J.F. High-resolution ground-based GPS measurements show intercampaign bias in ICESat elevation data near Summit, Greenland. *IEEE Trans. Geosci. Remote Sens.* **2011**, *49*, 3393–3400. [CrossRef]
46. Hansen, J.; Ruedy, R.; Sato, M.; Lo, K. Global surface temperature change. *Rev. Geophys.* **2010**, *48*. [CrossRef]
47. Tang, M.; Cheng, G.; Lin, Z. *Contemporary Climatic Variations over Qinghai-Xizang (Tibetan) Plateau and Their Influences on Environments*; Guangdong Science and Technology Press: Guangzhou, China, 1998.
48. Yang, W.; Guo, X.; Yao, T.; Zhu, M.; Wang, Y. Recent accelerating mass loss of southeast Tibetan glaciers and the relationship with changes in macroscale atmospheric circulations. *Clim. Dyn.* **2016**, *47*, 805–815. [CrossRef]
49. Song, C.; Ke, L.; Huang, B.; Richards, K.S. Can mountain glacier melting explains the GRACE-observed mass loss in the southeast Tibetan Plateau: From a climate perspective? *Glob. Planet. Chang.* **2015**, *124*, 1–9. [CrossRef]
50. Chang, C.P.; Harr, P.; Ju, J. Possible roles of Atlantic circulations on the weakening Indian monsoon rainfall-ENSO relationship. *J. Clim.* **2001**, *14*, 2376–2380. [CrossRef]
51. Goswami, B.N.; Madhusoodanan, M.S.; Neema, C.P.; Sengupta, D. A physical mechanism for North Atlantic SST influence on the Indian summer monsoon. *Geophys. Res. Lett.* **2006**. [CrossRef]
52. Li, J.; Wu, Z.; Jiang, Z.; He, J. Can global warming strengthen the East Asian summer monsoon? *J. Clim.* **2010**, *23*, 6696–6705. [CrossRef]
53. Castro-Díez, Y.; Pozo-Vázquez, D.; Rodrigo, F.; Esteban-Parra, M. NAO and winter temperature variability in southern Eurotablepe. *Geophys. Res. Lett.* **2002**, *29*. [CrossRef]
54. Lim, Y.-K. The East Atlantic/West Russia (EA/WR) teleconnection in the North Atlantic: Climate impact and relation to Rossby wave propagation. *Clim. Dyn.* **2015**, *44*, 3211–3222. [CrossRef]

55. Thompson, D.W.J.; Wallace, J.M. Regional climate impacts of the Northern hemisphere annular mode. *Science* **2001**, *293*, 85–89. [CrossRef] [PubMed]
56. Yin, Z.Y.; Lin, Z.; Zhao, X. Temperature anomalies in central and eastern Tibetan Plateau in relation to general circulation patterns during 1951–1993. *Int. J. Climatol.* **2000**, *20*, 1431–1449. [CrossRef]
57. Shaman, J.; Tziperman, E. The effect of ENSO on Tibetan Plateau snow depth: A stationary wave teleconnection mechanism and implications for the South Asian monsoons. *J. Clim.* **2005**, *18*, 2067–2079. [CrossRef]